

## Meter-Scale Plasma-Wakefield Accelerator Driven by a Matched Electron Beam

P. Muggli,<sup>1</sup> B. E. Blue,<sup>2</sup> C. E. Clayton,<sup>2</sup> S. Deng,<sup>1</sup> F.-J. Decker,<sup>3</sup> M. J. Hogan,<sup>3</sup> C. Huang,<sup>2</sup> R. Iverson,<sup>3</sup> C. Joshi,<sup>2</sup>  
T. C. Katsouleas,<sup>1</sup> S. Lee,<sup>1</sup> W. Lu,<sup>2</sup> K. A. Marsh,<sup>2</sup> W. B. Mori,<sup>2</sup> C. L. O'Connell,<sup>3</sup> P. Raimondi,<sup>3</sup>  
R. Siemann,<sup>3</sup> and D. Walz<sup>3</sup>

<sup>1</sup>University of Southern California, Los Angeles, California 90089, USA

<sup>2</sup>University of California, Los Angeles, California 90095, USA

<sup>3</sup>Stanford Linear Accelerator Center, Stanford, California 94309, USA

(Received 16 December 2003; published 30 June 2004)

A high-gradient, meter-scale plasma-wakefield accelerator module operating in the electron blowout regime is demonstrated experimentally. The beam and plasma parameters are chosen such that the matched beam channels through the plasma over more than 12 beam beta functions without spreading or oscillating over a range of densities optimum for observing both deceleration and acceleration. The wakefield decelerates the bulk of the initially 28.5 GeV beam by up to 155 MeV; however, particles in the back of the same beam are accelerated by up to 280 MeV at a density of  $1.9 \times 10^{14} \text{ cm}^{-3}$  as the wakefield changes sign.

DOI: 10.1103/PhysRevLett.93.014802

PACS numbers: 41.75.Ht, 41.75.Lx, 52.40.Mj

Plasma-based particle acceleration schemes [1] offer the possibility of accelerating charged particles to very high energies in a very short distance and thereby significantly reducing the size and cost of a future particle accelerator for high-energy physics. These schemes use ultraintense laser [2] or particle beams [3] as a source of free energy to excite the accelerating mode [a relativistic plasma wave (RPW)] in a plasma. Gradients in excess of 100 GeV/m over a few millimeters have been demonstrated using laser-driven RPWs [4–9]. Therefore, one of the key milestones in the realization of a high-energy plasma accelerator driven by laser or by particle beams is significantly increasing the length of the accelerator module [1]. For particle beam drivers, this needs to be achieved without significant transverse emittance growth. In this Letter, we present the first experimental demonstration of a meter-scale plasma-wakefield accelerator (PWFA) module that is driven by an intense, ultrarelativistic (28.5 GeV) electron beam. The beam and plasma parameters are chosen such that the beam propagates through the plasma with a constant radius (i.e., matched) with minimal emittance growth at densities near the optimum for acceleration. At the optimum density for observing maximum acceleration [10], the electrons in the head of the beam drive a nonlinear plasma wakefield in the electron blowout regime [10–12]. The wakefield decelerates the bulk of the incoming beam by up to 155 MeV; however, the particles in the back of the same beam are accelerated by up to 280 MeV as the wakefield changes sign. The accelerating gradient is roughly an order of magnitude larger than that in the 3 km long rf linear accelerator used to produce the drive beam. The results reported here represent a first step toward a recently proposed concept to increase the energy of a kilometers long linear collider by adding much shorter, but ultrahigh gradient plasma sections called afterburners [13].

Previous electron beam driven PWFA experiments have been performed with beams with energies on the order of 10 MeV in  $\approx 10$  cm long plasmas [14,15], thereby limiting the possibility of energy gain to typically a few MeV. Recently, a meter-scale PWFA module driven by a positron beam has been demonstrated [16]. However, the physics of wake excitation by an electron or a positron beam is different. In the electron beam driver case, the plasma electrons are expelled from the beam volume, the beam envelope experiences multiple betatron oscillations, and the wakefield can be highly nonlinear. In the case of a positron beam driver, the plasma electrons are pulled toward the beam volume, and no clear betatron oscillations of the beam envelope are expected. Also, the wake tends to be more sinusoidal with lower amplitude than that driven by an electron beam with otherwise similar parameters [16].

Figure 1 shows the experimental setup. The ultrarelativistic electron ( $e^-$ ) beam from the Stanford Linear Accelerator is delivered to the Final Focus Test Beam line [17] with  $N \approx 1.9 \times 10^{10}$  electrons per bunch at an energy of 28.5 GeV and a Gaussian bunch length with  $\sigma_z \approx 700 \mu\text{m}$  (or  $\sigma_z/c \approx 2.3$  ps). The incoming beam is focused near the entrance of the plasma, to a typical round, Gaussian size of  $\sigma_{r0} \approx 30 \pm 2 \mu\text{m}$ . The beam size before and after the plasma is monitored by imaging the optical transition radiation (OTR) emitted by single

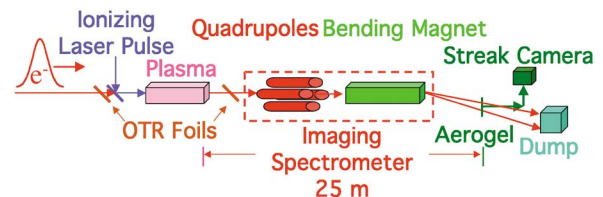


FIG. 1 (color). Schematic of the plasma-wakefield acceleration experimental setup (not to scale).

bunches when traversing  $\approx 37 \mu\text{m}$  thick titanium foils located approximately 1 m upstream and downstream from the plasma [18,19]. After exiting the plasma the beam travels through quadrupole and dipole (bending) magnets arranged in an imaging spectrometer configuration. The beam at the plasma entrance or at the plasma exit is imaged onto a  $\approx 1 \text{ mm}$  thick piece of aerogel located  $\approx 25 \text{ m}$  downstream from the plasma, where it emits Cherenkov radiation. The visible Cherenkov light is imaged onto the slit of a streak camera to disperse the energy spectrum of the bunch in time with a resolution of  $\approx 1 \text{ ps}$ . The spectrometer has an effective energy resolution of  $\approx 36 \text{ MeV}$  for a beam size of  $30 \mu\text{m}$  at the plasma exit.

The plasma is created through single photon ionization of lithium vapor contained in a heat-pipe oven [20]. The plasma column is  $\approx 1.4 \text{ m}$  long and has a typical transverse area of  $\approx 0.12 \text{ cm}^2$ . The plasma density  $n_e$  is proportional to the energy of the ionizing ( $\lambda = 193 \text{ nm}$ ) laser pulse and can be varied between 0 and  $\approx 2 \times 10^{14} \text{ cm}^{-3}$ . The value of  $n_e$  is calculated from laser energy absorption measurements and by fitting of an envelope model to the variations of the beam size observed as a function of the laser energy [21].

In the experiment reported here, the beam charge density  $n_b = N/[(2\pi)^{3/2}\sigma_z\sigma_{r0}] \approx 2.8 \times 10^{15} \text{ cm}^{-3}$  is much larger than the plasma density ( $n_b > n_e$ ), the transverse beam size is smaller than the plasma collisionless skin depth [ $\sigma_{r0} < c/\omega_p$ ,  $\omega_p = (n_e e^2/\epsilon_0 m_e)^{1/2}$  is the electron plasma angular frequency], and the experiment is thus performed in the nonlinear, blowout regime of the PWFA [10,12]. In this regime, the particles in the head of the bunch expel all the plasma electrons from the bunch volume and create a pure ion column, which exerts a strong focusing force on the remainder of the bunch as it propagates through the plasma. The expelled plasma electrons rush back on the beam axis, behind the bunch, and create an on-axis electron density spike which results in a highly nonlinear wakefield.

We have previously shown [21] that in this blowout regime, the beam envelope dynamics are well described by an envelope model for the transverse beam size  $\sigma_r(z)$ :  $\sigma_r''(z) + K\sigma_r(z) - \epsilon^2/\sigma_r^3(z) = 0$ . Here  $\epsilon$  is the beam emittance and  $K = eE_r/rm_e\gamma c^2 = \omega_p^2/2\gamma c^2$  is the plasma focusing strength resulting from the radial field of the pure ion column:  $E_r = (en_e/2\epsilon_0)r$ . A favorable situation is reached when the plasma and the beam are matched, which is achieved when the plasma focusing term  $K$  compensates for the beam divergence term arising from the finite beam emittance  $\epsilon$ , i.e., when  $K = \epsilon^2/\sigma_{r0}^4$ . In this case, the beam focused at the plasma entrance ( $\sigma_{r0}' = 0$ ) propagates along the plasma with a constant transverse size  $\sigma_{r0}$ , i.e., the beam size at the plasma entrance.

In this experiment, the matching condition corresponds to a beam spot size of  $33 \pm 3 \mu\text{m}$  for plasma densities in the range  $(1.2\text{--}2.5) \times 10^{14} \text{ cm}^{-3}$ . As shown in Fig. 2, the

beam size recorded on the downstream OTR screen oscillates as the plasma density increases from low densities ( $K < \epsilon^2/\sigma_{r0}^4$ ) toward the matched density ( $K \approx \epsilon^2/\sigma_{r0}^4$ ). The size of these oscillations decreases as the matching condition is approached. Indeed, the beam size remains almost constant as the beam density is varied from  $(1.3\text{--}1.9) \times 10^{14} \text{ cm}^{-3}$ , indicating that the beam is close to being matched to the plasma. Imaging the beam at the plasma exit for  $n_e > 7 \times 10^{13} \text{ cm}^{-3}$  thus preserves the overall energy resolution of the spectrometer and removes any contribution to the energy spectrum that could arise from a beam tail exiting the plasma with a transverse momentum [22].

The continuous curve shown in Fig. 2 is the result of the best fit of the envelope model to the experimental data and is a sensitive function of  $\sigma_{r0}$  and  $\epsilon$ , the beam parameters at the plasma entrance. In this experiment, the incoming beam beta function, the equivalent parameter to the Rayleigh length of a laser beam for a particle beam, is  $\beta_0 = \sigma_{r0}^2/\epsilon = 0.11 \text{ m}$ . Therefore, Fig. 2 shows that, at the highest densities, the matched beam is channeled over more than 12 beam beta functions. The agreement between the fit and the experimental data points on Fig. 2 shows that the transverse emittance of the beam is preserved for  $n_e = (0\text{--}1.8) \times 10^{14} \text{ cm}^{-3}$ .

In expelling the plasma electrons, the bunch electrons do work and therefore lose energy. However, as the plasma wavelength  $\lambda_p = 2\pi c/\omega_p$  approaches  $\sqrt{2}\pi\sigma_z$  (here for  $n_e > 1.4 \times 10^{14} \text{ cm}^{-3}$ , hereafter called the optimum density), the longitudinal component of the wakefield reverses sign within the bunch itself and can thus accelerate the electrons at the trailing end of the bunch. Single event, streak camera images of the beam dispersed in energy and time after interacting with a low

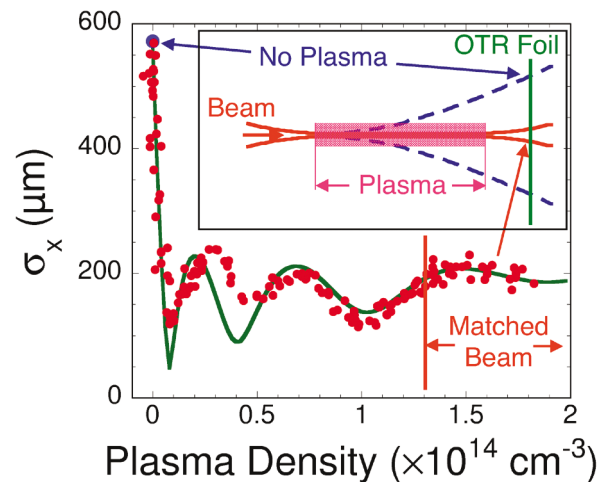


FIG. 2 (color). Transverse size  $\sigma_x$  of the beam (red points) in the  $x$  plane measured on the downstream OTR foil (see illustration inset) as a function of plasma density. The green line is the best fit to the data using a beam envelope model in which  $\sigma_{x0} = 30 \mu\text{m}$ ,  $\epsilon_x = 9 \times 10^{-9} \text{ m rad}$ , and  $\beta_0 = 0.11 \text{ m}$ .

( $n_e = 7 \times 10^{13} \text{ cm}^{-3}$ ) and a high ( $n_e = 1.9 \times 10^{14} \text{ cm}^{-3}$ ) density plasma are shown in Figs. 3(a) and 3(b). At the low density, where the energy loss of the beam is small, the streak camera image is dominated by the incoming beam correlated energy spread. The crosses on these images mark the mean energy of the 1 ps wide slice at the beam center at these two densities. Comparison between these two images shows that at high  $n_e$  the center slice of the beam loses  $\approx 170 \text{ MeV}$  energy, while the slices in the back of the beam gain energy.

Figure 3(c) shows the energy of the individual 1 ps wide beam slices, after summing typically ten individual streaks, at three different plasma densities. For these three values of  $n_e$  the electron beam size at the plasma exit (not shown) and therefore on the streak camera slit is almost constant. The beam's incoming energy chirp of  $\approx 480 \text{ MeV}$  is visible at  $n_e = 7 \times 10^{13} \text{ cm}^{-3}$  [Fig. 3(c), red diamonds]. This same chirp is also seen without plasma, when imaging the beam at the plasma entrance location. As  $n_e$  is increased to  $1.5 \times 10^{14} \text{ cm}^{-3}$  (green squares), one can clearly see that nearly all the slices lose energy to various degrees relative to the low  $n_e$  data. At  $n_e = 1.9 \times 10^{14} \text{ cm}^{-3}$ , the energy loss is greater; however, the last slice at +6 ps has, in fact, gained energy. Figure 3(c) shows that, at  $n_e = 1.9 \times 10^{14} \text{ cm}^{-3}$ , the maximum beam energy loss is 230 MeV for the 1 ps slice, and the energy gain is 85 MeV for the +6 ps slice.

Closer examination of Fig. 3(c) reveals that there is an apparent energy loss of  $\approx 50 \text{ MeV}$  at  $n_e = 1.9 \times 10^{14} \text{ cm}^{-3}$  for a beam slice at -5 ps (beam front). This is, however,  $\approx 5$  times larger than that predicted by the linear theory for wakes induced by Gaussian beams [23] and than that found in fully nonlinear 3D, particle-in-cell simulations of the experiments [24]. Therefore, it is reasonable to assume that the 50 MeV energy loss seen by the 5 ps slice at the head of the beam is due to a

$\approx 40 \mu\text{m}$  vertical deflection of the whole beam at the exit of the  $\approx 1.4 \text{ m}$  long plasma and that it is likely caused by the transverse density gradients in the plasma. We therefore assume that the slice at -5 ps at the front of the beam loses no energy for all events at a given density. The energy variations induced by the PWFA interaction [see Fig. 4(a)] are obtained by first averaging all the streaks at a given density and then by subtracting slice-by-slice energies measured at  $n_e \approx 7 \times 10^{13} \text{ cm}^{-3}$  [Fig. 3(c)] from the energies measured at higher densities. This procedure leaves a 45 MeV systematic experimental error on the energy change of individual slices.

At  $n_e = 1.5 \times 10^{14} \text{ cm}^{-3}$  [green squares, Fig. 4(a)], almost all slices of the bunch lose energy. The peak energy loss is  $\approx 115 \text{ MeV}$  at  $\approx +1 \text{ ps}$  (relative to the bunch centroid). At this low density the wake wavelength is long compared to the value optimum for acceleration ( $\lambda_p \approx \sqrt{2}\pi\sigma_z$ ), and no significant energy gain is expected or observed. At  $n_e = 1.9 \times 10^{14} \text{ cm}^{-3}$  (blue circles) the peak energy loss is larger,  $\approx 155 \text{ MeV}$  and occurs earlier in the bunch ( $\approx -1 \text{ ps}$ ) because the plasma wavelength is shorter. Simultaneously, two later slices of the beam (+5 and +6 ps) gain energy with a maximum slice average energy gain of about  $\approx 156 \text{ MeV}$  observed for the +6 ps slice. The number of accelerated electrons in this 1 ps slice of the Gaussian beam is  $\approx 1.4 \times 10^8$ .

The individual energy distributions of electrons in the last picosecond slices of Fig. 3 (see the vertical white lines at +5.5 ps) are examined further in Fig. 4(b). The distributions for the  $n_e = 7 \times 10^{13} \text{ cm}^{-3}$  (blue circles) where energy gain is neither expected nor observed, and  $n_e = 1.9 \times 10^{14} \text{ cm}^{-3}$  are shown (red squares). At  $n_e = 1.9 \times 10^{14} \text{ cm}^{-3}$ , the full width at half maximum (FWHM) of this distribution is 280 MeV wider than the FWHM of the distribution for  $n_e = 7 \times 10^{13} \text{ cm}^{-3}$ . Therefore, some electrons have gained at least 280 MeV

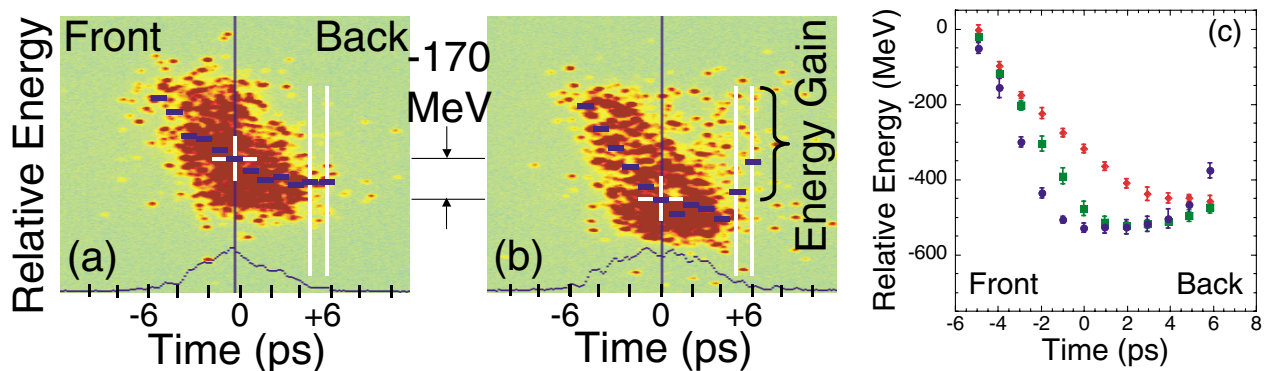


FIG. 3 (color). Streak camera images of a single electron bunch dispersed in time and energy after propagation through (a) low density ( $n_e = 7 \times 10^{13} \text{ cm}^{-3}$ ) and (b) high density ( $n_e = 1.9 \times 10^{14} \text{ cm}^{-3}$ ) plasma (see text for details). The blue tick marks show the mean energy of picosecond wide slices of the beam. (c) Relative energy of the mean position of a picosecond wide slice of the beam vs time calculated from the streak camera images for three different plasma densities:  $n_e = 7 \times 10^{13} \text{ cm}^{-3}$  (red diamonds),  $n_e = 1.5 \times 10^{14} \text{ cm}^{-3}$  (green squares), and  $n_e = 1.9 \times 10^{14} \text{ cm}^{-3}$  (blue circles). The curves are an average of  $\approx 10$  events such as those shown in (a) and (b). The error bar (rms of the data) shows the vertical jitter in the data.

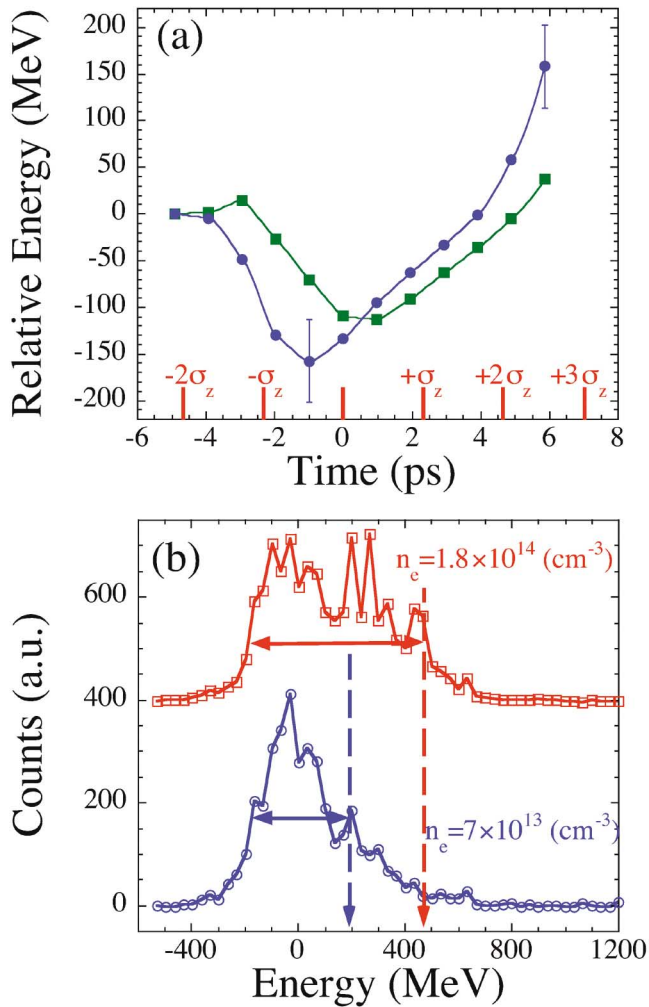


FIG. 4 (color). (a) Relative energy variations experienced by the mean of 1 ps wide slices of the beam fitted with a Gaussian distribution at  $n_e = 1.5 \times 10^{14} \text{ cm}^{-3}$  (green squares) and  $n_e = 1.9 \times 10^{14} \text{ cm}^{-3}$  (blue circles). These curves are obtained by averaging  $\approx 10$  individual streaks after lining up the first slice ( $-5$  ps) to remove any vertical pointing jitter of the beam. The uncertainty on the slice timing (not shown) is  $<0.5$  ps. (b) Relative energy distribution of the picosecond slice at  $+5.5$  ps for  $n_e = 7 \times 10^{13} \text{ cm}^{-3}$  (blue circles) and  $n_e = 1.9 \times 10^{14} \text{ cm}^{-3}$  (red squares, shifted vertically). The horizontal arrows are the full widths at half maximum of the distributions.

energy at the higher density, consistent with approximately 290 MeV seen in 3D particle-in-cell code simulations of this experiment using the code OSIRIS [24,25]. The peak gradient over the 1.4 m long plasma is thus 200 MeV/m.

Finally, according to theory, the accelerating gradient in a PWEA scales approximately as  $N/\sigma_z^2$ , the number of particles in the bunch divided by the square of the bunch length [11,23]. Reducing the bunch length by a factor of 10 is thus expected to bring the accelerating gradient in the 20 GeV/m range for the same beam charge and at an appropriately optimized plasma density. Such large gradients are necessary to realize the recently proposed scheme to double the energy of a linear collider by placing few meters long, ultrahigh gradient plasma sections just before the interaction point-A Plasma Afterburner [13].

This work is supported by the U.S. DoE Grants No. DE-FG03-92ER40745, No. DE-AC03-76SF00515, No. DE-FG03-98DP00211, No. DE-FG03-92ER40727, and No. DE-AC-03-76SF0098, and NSF Grants No. ECS-9632735, No. MS-9722121, and No. PHY-0078715. Dr. P. Tsou from JPL provided the aerogel.

- 
- [1] T. Tajima and J.M. Dawson, Phys. Rev. Lett. **43**, 267 (1979).
  - [2] C. Joshi *et al.*, Nature (London) **311**, 525 (1984).
  - [3] P. Chen *et al.*, Phys. Rev. Lett. **54**, 693 (1985).
  - [4] D. Gordon *et al.*, Phys. Rev. Lett. **80**, 2133 (1998).
  - [5] A. Modena *et al.*, Nature (London) **377**, 606 (1995).
  - [6] V. Malka *et al.*, Science **298**, 1596 (2002).
  - [7] A. Ting *et al.*, Phys. Rev. Lett. **77**, 5377 (1996).
  - [8] W. Leemans *et al.*, Phys. Rev. Lett. **89**, 174802 (2002).
  - [9] D. Umstadter *et al.*, Science **273**, 472 (1996).
  - [10] T. Katsouleas *et al.*, Part. Accel. **22**, 81 (1987).
  - [11] C. Joshi *et al.*, Phys. Plasmas **9**, 1845 (2002).
  - [12] J.B. Rosenzweig *et al.*, Phys. Rev. A **44**, R6189 (1991).
  - [13] S. Lee *et al.*, Phys. Rev. ST Accel. Beams **5**, 011001 (2002).
  - [14] N. Barov *et al.*, Phys. Rev. Lett. **80**, 81 (1998).
  - [15] N. Barov *et al.*, Phys. Rev. ST Accel. Beams **3**, 011301 (2000).
  - [16] B. Blue *et al.*, Phys. Rev. Lett. **90**, 214801 (2003).
  - [17] V. Balakin *et al.*, Phys. Rev. Lett. **74**, 2479 (1995).
  - [18] M. Hogan *et al.*, Phys. Plasmas **7**, 2241 (2000).
  - [19] P. Catravas *et al.*, Phys. Rev. E **64**, 046502 (2001).
  - [20] P. Muggli *et al.* IEEE Trans. Plasma Sci. **27**, 791 (1999).
  - [21] C.E. Clayton *et al.*, Phys. Rev. Lett. **88**, 154801 (2002).
  - [22] A. Geraci and D.H. Whittum, Phys. Plasmas **7**, 2241 (2000); B.E. Blue, Master's thesis, University of California, Los Angeles, 2000.
  - [23] W. Lu *et al.* (to be published).
  - [24] S. Deng *et al.*, in *Advanced Accelerator Concepts, Tenth Workshop*, edited by C. Clayton and P. Muggli, AIP Conf. Proc. No. 647 (AIP, New York, 2002), p. 592.
  - [25] S. Lee *et al.* Phys. Rev. E **61**, 7014 (2000).